NOLTA, IEICE

Paper

Self-organizing striped and spotted patterns on a discrete reaction-diffusion model

Tetsuya Asai [1 a)] *and Ikuko N. Motoike* [2]

[1] *Graduate School of Information Science and Technology, Hokkaido University, Kita 14, Nishi 9, Sapporo 060-0814, Japan*

[2] *PRESTO, Japan Science and Technology Agency (JST), 4-1-8 Honcho Kawaguchi, Saitama 332-0012, Japan*

[a)] *asai@ist.hokudai.ac.jp*

Abstract: We propose a novel and simple discrete reaction-diffusion model that self-organizes striped and spotted spatial patterns. Through theoretical analyses, we show that the spatial frequency of the generated patterns is proportional to diffusion length. Through extensive numerical simulations, we demonstrate that the model can produce Turing-like striped and spotted spatial patterns.

Key Words: Turing patterns, reaction-diffusion systems, image processing

1. Introduction

Self-organizing striped and spotted spatial patterns can be observed everywhere in nature, *e.g.*, animal's or tropical fish's skin surface as well as human fingerprints, bacterial colony, artificial nanocrystals, and so on [1]. Alan Turing introduced a concept of "diffusion-driven instability" for these phenomena where diffusion enhances transition from a homogeneous state to a spatially inhomogeneous stable state and time development in systems undergoing this transition is described by the sum of reaction and diffusion [2]. The transition relates to the local production/extinction of the substance or state, and the time development for this transition relates to a transport process that tends to dampen any inhomogeneity of the neighboring region; the system undergoing transition is referred to as the reaction-diffusion (RD) system [3–5]. Turing proposed a model where the spatial homogeneous structure could exhibit spatial instability with the addition of the diffusion effect. A well-known feature of the "Turing model" is that it exhibits striped or spotted patterns that are self-organized at the equilibrium [6–8].

Based on the Turing model, a discrete RD model that generates Turing-like patterns has been proposed, in which, discrete dynamics for diffusion between chemical substances is introduced and all the states (usually represented by two variables, activators and inhibitors) are represented by a single binary variable [9]. In a previous report, we proposed an extended model where the spatial diffusion of activators and inhibitors is described by time-dependent diffusion equations but the temporal update for every cycle is determined by a discrete dynamics [10]. In this report, we propose the improved model where the diffusion is described by simple "time-independent" instant diffusion and provide a

[Received: September 2, 2010. Revised: January 17, 2011. Published: July 1, 2011.]
[DOI: 10.1588/nolta.2.363]
Nonlinear Theory and Its Applications, IEICE, vol. 2, no. 3, pp. 363–371

theoretical analysis as well as extensive numerical simulation results.

2. The model

Let us start by introducing a resistor ladder model, shown in Fig. 1(a). The i-th node equation is given by

$$\frac{u_{i-1} + u_{i+1} - 2u_i}{R} - g(u_i - V_i) = 0, \tag{1}$$

where u_i represents the i-th node potential; R, the horizontal resistance; g, the vertical conductance; and V_i, the input voltage of the i-th node. For 2-D resistive materials, as shown in Fig. 1(b), one may obtain the continuous form

$$D\nabla^2 u(x) - g[u(x) - V(x)] = 0, \tag{2}$$

where x is the space; $u(x)$, the potential distribution; $\nabla = \partial/\partial x$; $V(x)$, the input potential distribution; and D, the diffusion coefficient ($\equiv \Delta x^2/R$, $\Delta x \ll 1$). Obviously, if we apply input $V(x)$ to the bottom surface of the resistive material, the diffused distribution $[u(x)]$ is observed on the top surface. We employ this continuous resistive material to express "instant" diffusion of chemicals.

By introducing the following Fourier transformation

$$\tilde{u}(k) \equiv \int_{-\infty}^{\infty} u(x)\mathrm{e}^{-ikx}dx, \qquad u(x) \equiv \frac{1}{2\pi}\int_{-\infty}^{\infty} \tilde{u}(k)\mathrm{e}^{ikx}dk, \tag{3}$$

we obtain the response function of the resistive material [for $V(x) = \delta(x)$, where $\delta(x)$ represents the delta function] as

$$\tilde{u}(k) = \frac{\alpha^2}{k^2 + \alpha^2}, \text{ where } \alpha \equiv \sqrt{\frac{g}{D}}. \tag{4}$$

The inverse Fourier transformation of $\tilde{u}(k)$ represents the impulse response of the resistive material. To obtain this, one may use the residue theorem with the following formula:

$$\int_{-\infty}^{\infty} \frac{1}{k^2 + \alpha^2}dk = \frac{\pi}{\alpha}e^{-\alpha|x|}. \tag{5}$$

The resulting impulse response is

$$u(x) = \frac{1}{2}\alpha\mathrm{e}^{-\alpha|x|}. \tag{6}$$

Now, we consider two resistive ladder networks coupled with each other [Fig. 2(a)]. Each ladder accepts common input voltage V_i^t at time t. The continuous model is shown in Fig. 2(b). Here, we assume that i) $R_u > R_v$ and ii) the continuous system calculates the differential voltages between $u(x)$ and $v(x)$ at time t. Consequently, the impulse response is given by

$$\mathrm{DoE}(x) \equiv \frac{1}{2}\left(\alpha_u\mathrm{e}^{-\alpha_u|x|} - \alpha_v\mathrm{e}^{-\alpha_v|x|}\right), \text{ where } \alpha_{u,v} \equiv \sqrt{\frac{g_{u,v}R_{u,v}}{\Delta x^2}} \tag{7}$$

and $\mathrm{DoE}(x)$ denotes the "Difference of Exponentials" kernel. The differential voltage distribution between $u(x)$ and $v(x)$ for given $V^t(x)$ is thus obtained by calculating the following convolution:

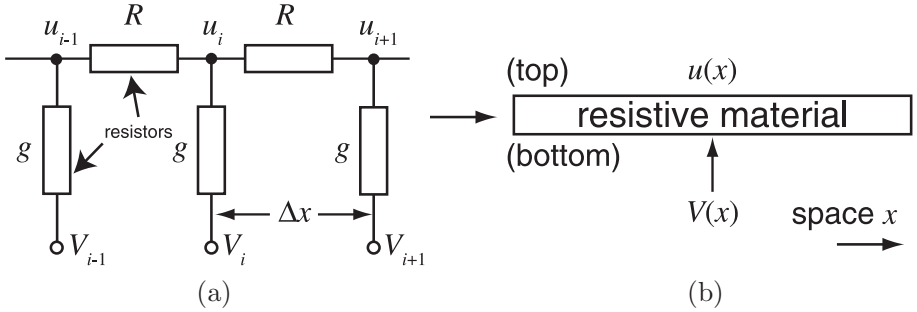

Fig. 1. Discrete resistive ladder and continuous resistive material.

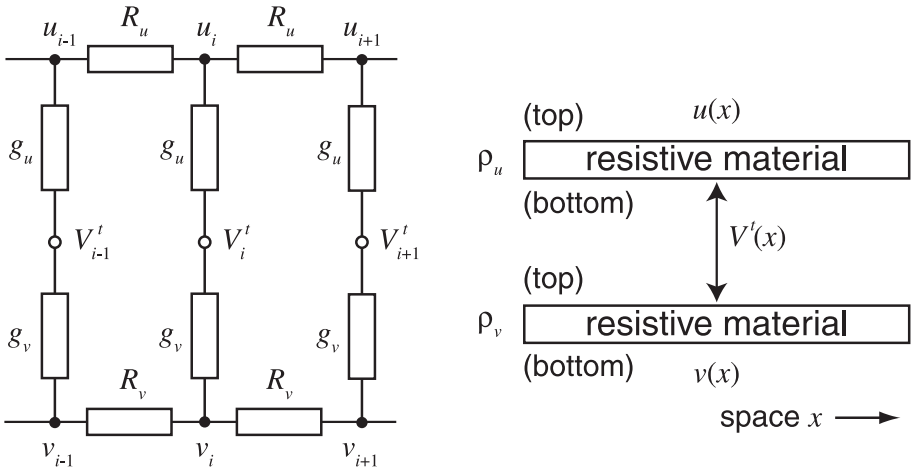

(a) (b)

Fig. 2. Network of two resistive ladders and continuous resistive model.

$$z^t(x) = \int_{-\infty}^{\infty} V^t(x - X) \cdot \mathrm{DoE}(X)\, dX. \tag{8}$$

Here, let us introduce the following discrete dynamics for this DoE system:

$$V^{t+1}(x) = \Theta[z^t(x)], \tag{9}$$

where $\Theta(\cdot)$ is the piecewise linear function defined by

$$\Theta(x) \equiv \begin{cases} 1 & (x > 2/\beta) \\ \beta x/4 + 0.5 & (-2/\beta \le x \le 2/\beta) \\ 0 & (x < -2/\beta), \end{cases} \tag{10}$$

where β represents the slope gain.

When an initial step input, $V^0(x) = \theta(x)$ [$\theta(\cdot)$: step function], is applied to the system, we obtain

$$z^0(x) = \int_0^{\infty} \mathrm{DoE}(x - X)\, dX = \begin{cases} (-\mathrm{e}^{-\alpha_u x} + \mathrm{e}^{-\alpha_v x})/2\,, & (x > 0) \\ (\mathrm{e}^{\alpha_u x} - \mathrm{e}^{\alpha_v x})/2 \quad , & (x < 0) \end{cases}. \tag{11}$$

Figure 3(a) plots the initial (step) input and the resulting $z^0(x)$ (diffused differential output). $V^1(x)$, where $z^0(x) \ge 2/\beta$ (or $z^0(x) \le -2/\beta$), is 1 (or 0), whereas $V^1(x)$, where $-2/\beta < z^0(x) < 2/\beta$, is between $(0, 1)$, as shown in Fig. 3(b). We reiterate that this $V^1(x)$ is applied to the system to calculate subsequent $z^1(x)$. Obviously, regions of $V^1(x)$ where $z^0(x) \in 0, 1$ are stable for the subsequent update, and hence, the boundary condition that represents the stable regions is $|z^0(x)| \ge 2/\beta$. When we

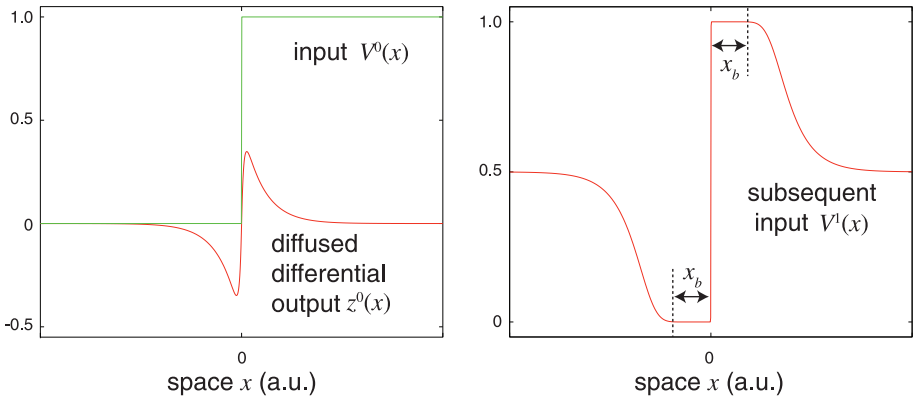

(a) (b)

Fig. 3. Responses of 1-D network model with step input.

assume $\alpha_u \gg \alpha_v$ ($e^{-\alpha_u x} \ll e^{-\alpha_v x}$ for $x > 0$), we obtain the approximated boundary [x_b in Fig. 3(b)] as

$$x_b \approx \alpha_v^{-1} \ln \frac{\beta}{4}. \tag{12}$$

Since this process is repeated in the subsequent steps, the equilibrium spatial frequency [of $V^\infty(x)$] is given by $(2x_b)^{-1}$, which indicates that the spatial frequency is proportional to $\alpha_v \sim \sqrt{g_v R_v}$ (diffusion length of resistive material v) when $R_u \gg R_v$.

3. Simulation results

In the following simulations, instead of using α_u and α_v as diffusion length parameters, we use the following diffusion coefficients:

$$D_u = \frac{g_u}{\alpha_u^2}, \qquad D_v = \frac{g_v}{\alpha_v^2}. \tag{13}$$

Figure 4 shows numerical results of the proposed 1-D model with an initial step input. Several iterations are plotted ($t = 0, 1, \cdots, 5$). In the simulations, the following parameter values were used: $\Delta x = 0.02$, $g_u = g_v = 1$, $\beta = 10^3$, $D_u = 10^{-3}$, and $D_v = 1$, with Neumann boundaries. In this figure, the plots of initial step input $V^0(x)$ at $t = 0$, diffused and subtracted output $z^0(x)$ at $t = 0$, and

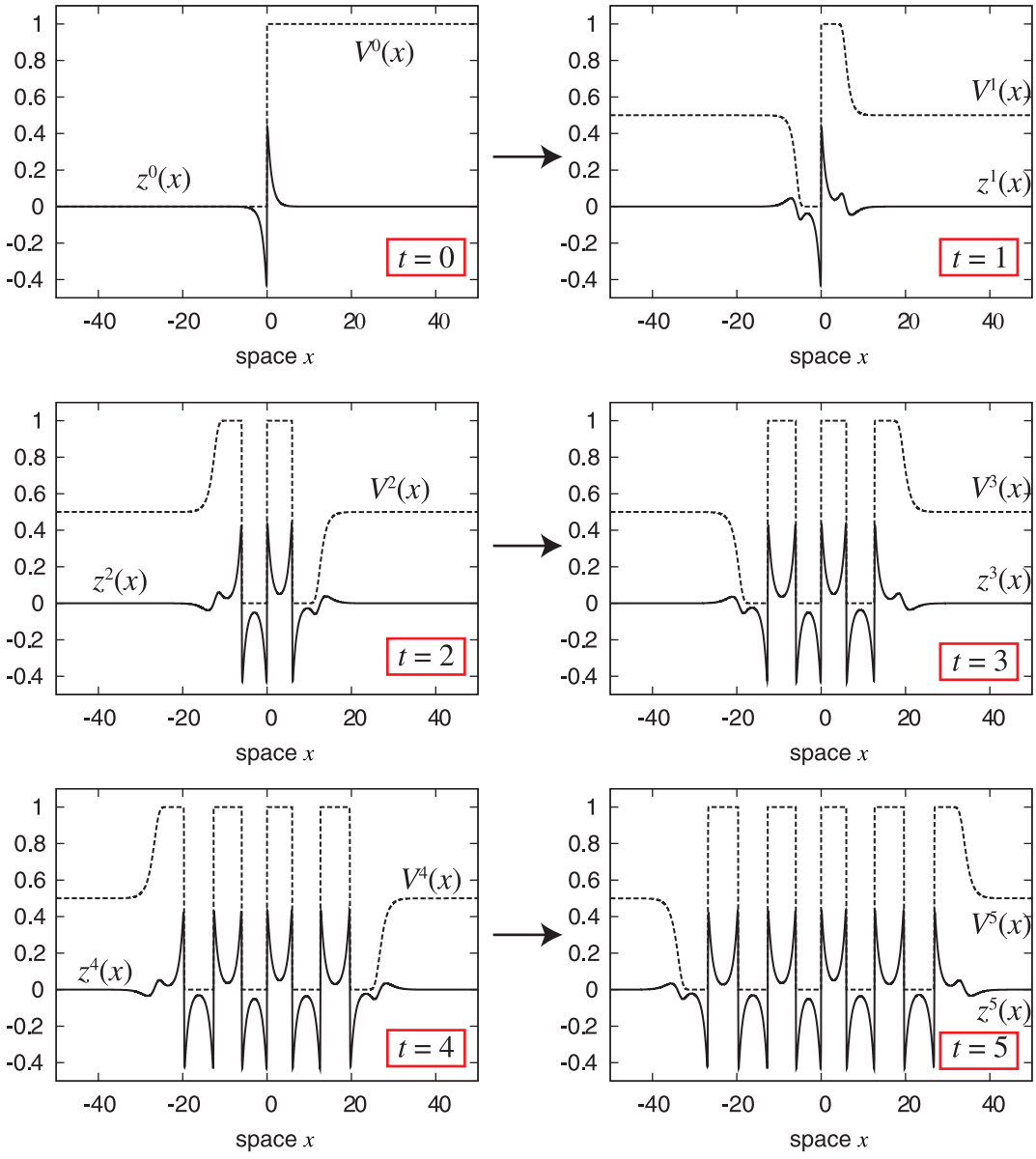

Fig. 4. Time evolution of 1-D network with step input.

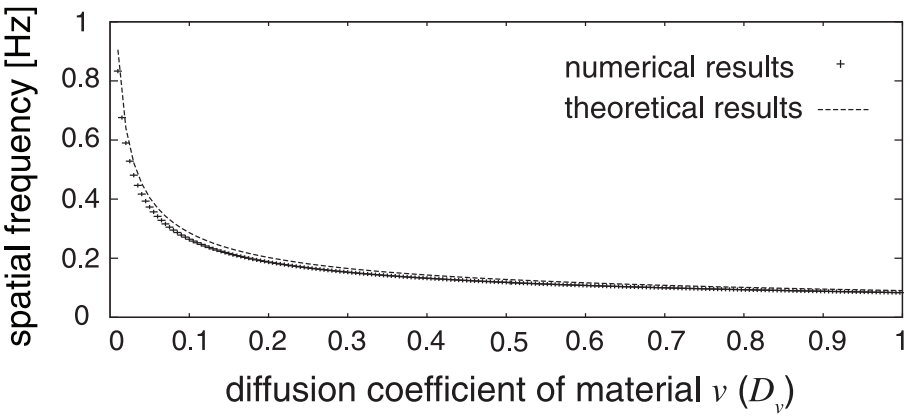

Fig. 5. Dependence of the frequency on diffusion coefficient D_v. The dashed-line represents the theoretical values, and the (+) line represents the numerical data.

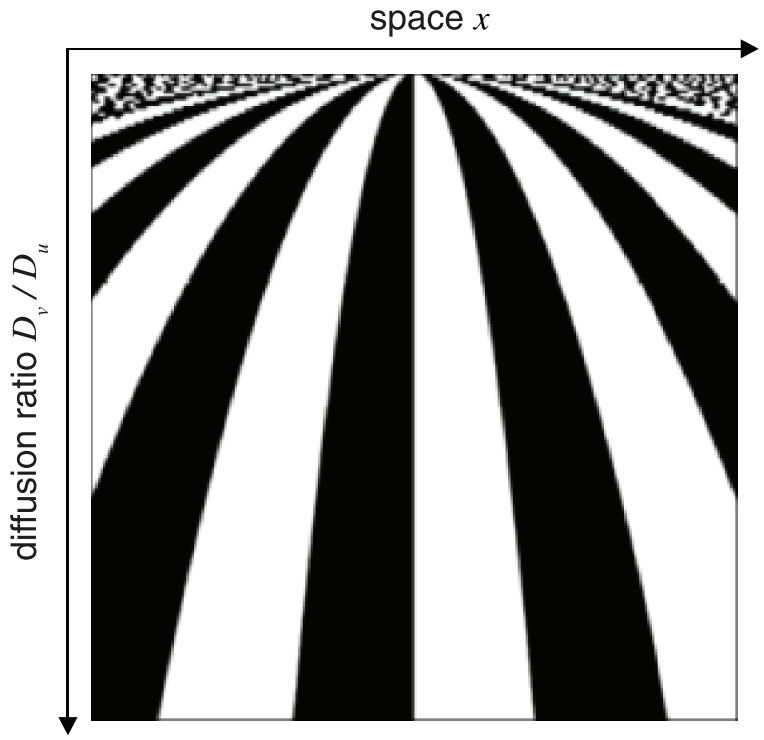

Fig. 6. Dependence of diffusion coefficients on generated 1-D spatial patterns with step input.

subsequent input $V^1(x)$ [to calculate $z^1(x)$] at $t = 1$ are exactly the same as plots in Fig. 3. When input $V^1(x)$ was applied, the system produced $z^1(x)$ at $t = 1$. This $z^1(x)$ was used to calculate the subsequent input $V^2(x)$ at $t = 2$. This operation was repeated until equilibrium. It should be noted that regions of $V^1(x) \in 0, 1$ were stable (were not updated) in the subsequent update operations, as explained before. Therefore the region boundary ($x = 0$ to x_b) determines the wavelength (spatial frequency).

Figure 5 shows the plotting of the spatial frequencies of the generated patterns obtained by numerical simulations and theoretical results ($f = (2x_b)^{-1}$). The theoretical results agreed well with the simulation results when $D_v \gg 0$. To obtain the theoretical spatial frequency, we assumed $\alpha_u \gg \alpha_v$ (this corresponds to $D_u \ll D_v$), as described above. In the simulation, D_u was set at 10^{-3}. Therefore, as $D_v \to 0$, differences between the numerical and theoretical results expands.

Figure 6 exhibits equilibrium pattern distributions of the model generated from the same initial (step) inputs as in Fig. 5, with various values of D_v/D_u and large x ($x = [-16, 16]$, $d = 1$, $D_u = 10^{-3}$, and $D_v = [5{\times}10^{-3}, 10^0]$). The black and white areas represent regions of $u = 1$ and $u = 0$, respectively.

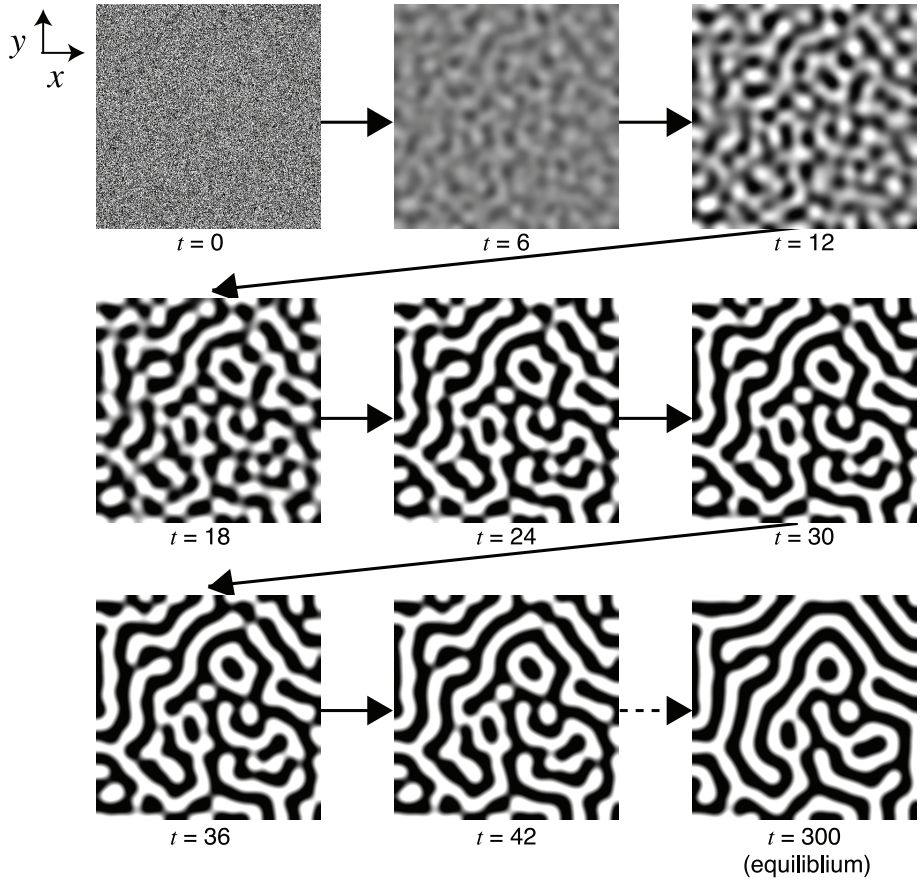

Fig. 7. Snapshots of striped patterns on 2-D model with random initial distribution.

As D_v/D_v increased, spatial frequencies of the generated patterns decreased, as expected.

We expanded the model to a 2-D system and performed numerical simulations. In the simulations, we used the alternating direction implicit (ADI) method with $\Delta x = \Delta y = 0.02$ and Neumann boundary conditions at the edge of the frame. The result is shown in Fig. 7 ($D_v/D_u = \beta = 10$ and $x = y = [0, 9.6]$). The initial state $[V^0(x, y)]$ was randomly set within $[0, 1]$. Each snapshot represents 2-D distributions of $V^t(x, y)$ ($V^t = 0$: black, $V^t = 1$: white). The first eight snapshots were taken after every 6 steps, and the final (equilibrium) shot was taken at step 300. The state of the patterns was rapidly changed to a quasi-stable state in the first several tens of steps and then shifted to stable state gradually. At the equilibrium, the space was filled with striped patterns that reflected the initial spatial distribution.

Our previous model was known to generate 2-D striped and spotted patterns when offset values of the sigmoidal response function had a nonzero value [10]. We here examine whether the same type of patterns can be observed in the present model. To do this, we modify our dynamics of Eq. (9) as

$$V^{t+1}(x) = \Theta[z^t(x) - c], \tag{14}$$

where c represents the offset value. Physically, c represents a total balance of the diffused activator ($\equiv u$) and inhibitor chemicals ($\equiv v$). When $c > 0$, v is predominant over u because the values of u must be larger than those of $v + c$ to ensure $\Theta(z^t(x) - c) > 0.5$, where $z^t(x)$ is proportional to $u - v$ at position x, and vice versa when $c < 0$. This can easily be confirmed from Fig. 8; the area occupied by inhibitors (black areas) is equal to the area occupied by activators (white) when $c = 0$, while inhibitors (black areas) become predominant as c increases or decreases ($c = [-0.12, 0.12]$ and $V^0(x, y)$ was randomly set within $[0, 1]$).

Finally, we introduce a possible application for the proposed system. A reaction-diffusion-based image restoring has been demonstrated in [10–12] where noisy images were restored without paying much attention to noise cleaning, contrast enhancement, and statistical (intelligent) compensation of

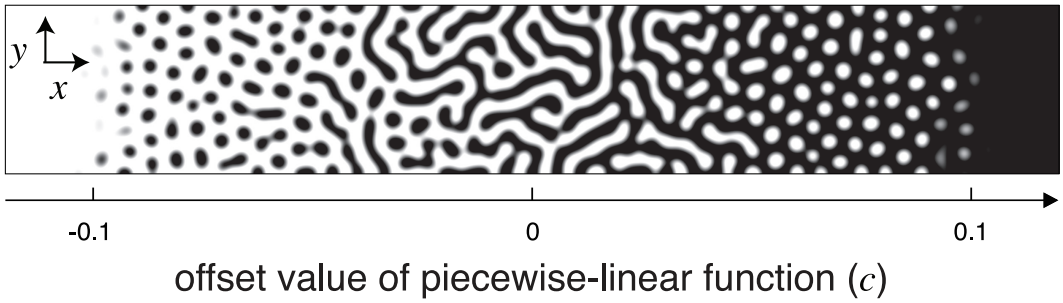

Fig. 8. Dependence of offset value in amplification on generated 2-D spatial patterns with random initial distribution.

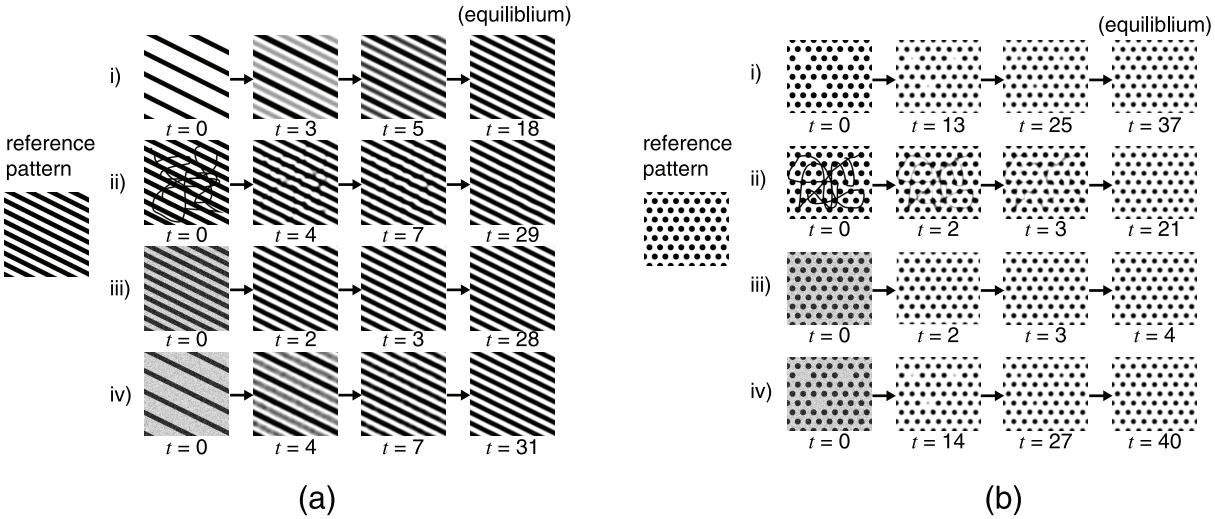

Fig. 9. Examples of the image restoration process using proposed 2-D system.

missing stripes and spots. Here, we try to demonstrate this type of image restoring on our system. Figure 9 shows examples of image restoration using the proposed system. During the simulations, we first created two types of reference images (striped and spotted references), as shown in Fig. 9(a) left and (b) left. Spatial (peak) frequencies of the reference images were set at the same frequency as that estimated by Eq. (12) for a given diffusion length of the system. Next, we broke the reference images into four types by i) removing some localizations from the reference image, ii) adding scratch noises on the reference, iii) adding Gaussian noises on the reference, and iv) removing some localizations and adding Gaussian noises simultaneously, as shown in Fig. 9 [i–iv]. The broken striped images were given to the system ($c = 0$) as the initial value $[V^0(x, y)]$, whereas the broken spotted images were given to the system ($c = 0.1$) as the initial value. As shown in pattern transitions in Fig. 9, all the broken patterns were successfully repaired along with the surrounding global striped and spotted patterns. Therefore, this system would be suitable for restoring almost-regularly-arranged striped and spotted patterns such as fingerprints and polka-dot patterns. To confirm this in practical environment, we employ a noisy fingerprint pattern as an input image. Figure 10(a) shows the results $[D_v/D_u = 10^{-1}/10^{-2}, \beta = 10, x = y = [0, 13], \Delta x = \Delta y = 0.02$ (650×650 pixels)]. The image restoring process was the same as in Fig. 9(a) where noisy local stripes were restored by surrounding global striped patterns. The system required around 100 updates until it reached equilibrium, to restore the fingerprint patterns. Around the boundaries (top, bottom, left, and right boundaries) of each snapshot, the generated (restored) pattern was distorted due to the Neumann boundary conditions. The initial pattern ($t = 0$) was superimposed on the equilibrium pattern ($t = 100$), as shown in Fig. 10(b). The black and red pixels represent the initial and equilibrium pixels, respectively. From this figure, one may see that red stripes were invented based on the pixel placement of the initial (black) pixels.

The image-restoring system shown in [10] had a Gaussian-shaped impulse response for diffusion

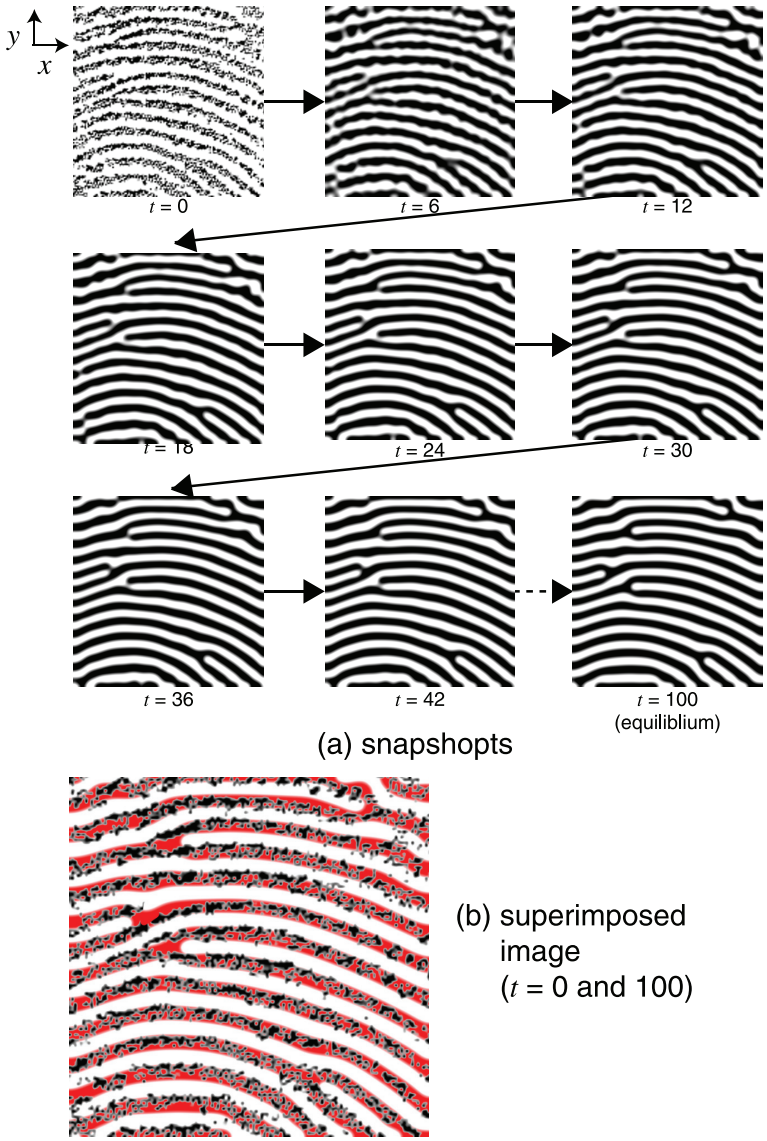

Fig. 10. Examples of fingerprint image restoration.

where the variance was controlled by time (which we call "time-dependent" diffusion), whereas the proposed system had a stiff impulse response given by (6) for instant diffusion, where the diffusion length was controlled by the resistance (which we call "time-independent" diffusion). Hence, there exists a qualitative difference of image-restoring performance between our previous system [10] and the proposed system. The most significant difference is the number of update steps to reach equilibrium. For example, our previous system required around 50 updates for fingerprint image restoration, but each update required 80 (for activators) plus 80 (for inhibitors) sub-updates for diffusion, which resulted in 8,000 updates to reach its equilibrium. On the other hand, thanks to the instant diffusion, the proposed system required around 100 updates until it reached to the equilibrium [Fig. 10(a)], which indicates that the proposed system is 80 times faster than our previous system, if the proposed model was implemented by the same fabrication process in [10]. The other important difference is the hardware scale. Our previous system required many local capacitors for computation of "time-dependent" diffusion, and they mainly occupied the chip area. However, the proposed model was intended to use two-layered resistive materials, hence the first and second layers of resistive poly-silicon in standard CMOS LSI can be used for computation of "time-independent" diffusion, which decrease the pixel area significantly. According to our brief estimation, the pixel area shown in [10] could be reduced by 80%, if the proposed model was implemented by using the same fabrication process. It would be more practical if the model was implemented on a chip with on-chip capacitive

sensor array devices (*e.g.*, [13, 14]).

4. Summary

We proposed a novel and simple reaction-diffusion (RD) model that can be developed using two-layered resistive materials with nonlinear differential amplifiers. Nominal resistive materials were employed to imitate the chemical diffusion of activators and inhibitors of the Turing system. Through theoretical analyses, we proved that spatial frequencies of the generated patterns were proportional to diffusion length of the resistive material. We then demonstrated that i) the model had the ability to produce Turing-like spatial patterns and ii) the model was able to reconstruct a striped or spotted image even if the initial (given) input image was damaged by external noises, scratches, and so on, by extensive numerical simulations. The results showed that even an instant diffusion of activators and inhibitors with amplification was able to account for the self-organizing striped and spotted patterns; these results may be useful to explain reasons for the existence of such patterns in various systems, by taking into account of the abstract (nominal-instant) diffusion of activator- and inhibitor-equivalent chemicals and the (autocatalytic) amplification.

Acknowledgments

This study was supported by a Grant-in-Aid for Scientific Research on Innovative Areas [20111004] from the Ministry of Education, Culture Sports, Science and Technology (MEXT) of Japan.

References

[1] P. Ball, *The Self-Made Tapestry: Pattern Formation in Nature*, Oxford University press, Oxford, 2001.

[2] A. M. Turing, "The chemical basis of morphogenesis," *Phil. Trans. R. Soc. Lond. B*, vol. 237, pp. 37–72, 1952.

[3] G. Nicolis and I. Prigogine, *Self-organization in Nonequilibrium Systems — From Dissipative Structures to Order through Fluctuations*, John Wiley & Sons, Inc., New York, 1977.

[4] I. Epstein and J. Pojman, *An introduction to nonlinear chemical dynamics*, Oxford University press, Oxford, 1998.

[5] A. De Wit, *Spatial patterns and spatiotemporal dynamics in chemical systems*, *Adv. Chem. Phys.*, vol. 109, pp. 435–513, 1999.

[6] Q. Ouyang and H.L. Swinney, "Transition from a uniform state to hexagonal and striped Turing patterns," *Nature*, vol. 353, pp. 610–612, 1991.

[7] J.D. Murray, *Mathematical Biology II (3rd Ed.)*, Chap. 2, p. 75, Springer, New York, 2002.

[8] Y.-N. Wu, P.-J. Wang, C.-J. Hou, C.-S. Liu, and Z.-G. Zhu, "Turing patterns in a reaction-diffusion system," *Commun. Theor. Phys.*, vol. 45, no. 4, pp. 761–764, 2006.

[9] D.A. Young, "A local activator-inhibitor model of vertebrate skin patterns," *Math. Biosci.*, vol. 72, pp. 51–58, 1984.

[10] Y. Suzuki, T. Takayama, I.N. Motoike, and T. Asai, "Striped and spotted pattern generation on reaction-diffusion cellular automata," *Int. J. Unconventional Computing*, vol. 3, no. 5, pp. 1713–1719, 2007.

[11] A. Sherstinsky and R.W. Picard, "M-lattice: from morphogenesis to image processing," *IEEE Trans. Image Processing*, vol. 5, no. 7, pp. 1137–1149, 1996.

[12] K. Ito, T. Aoki, and T. Higuchi, "Fingerprint restoration using digital reaction-diffusion system and its evaluation," *IEICE Trans. Fundamentals*, vol. E86-A, no. 8, pp. 1916–1924, 2003.

[13] S. Shigematsu, H. Morimura, Y. Tanabe, T. Adachi, and K. Machida, "A single-chip fingerprint sensor and identifier," *IEEE J. Solid-State Circuits*, vol. 34, no. 12, pp. 1852–1859, 1999.

[14] H. Morimura, S. Shigematsu, and K. Machida, "A novel sensor cell architecture and sensing circuit scheme for capacitive fingerprint sensors," *IEEE J. Solid-State Circuits*, vol. 35, no. 5, pp. 724–731, 2000.